

 Open access • Journal Article • DOI:10.1002/JMRI.26034

Improving lymph node characterization in staging malignant lymphoma using first-order ADC texture analysis from whole-body diffusion-weighted MRI.

— [Source link](#) 

[Katja N. De Paepe](#), [Frederik De Keyzer](#), [Pascal Wolter](#), [Oliver Bechter](#) ...+5 more authors

Institutions: [Katholieke Universiteit Leuven](#)

Published on: 01 Oct 2018 - [Journal of Magnetic Resonance Imaging](#) (J Magn Reson Imaging)

Topics: [Body region](#) and [Population](#)

Related papers:

- [Diagnostic value of diffusion-weighted magnetic resonance imaging: differentiation of benign and malignant lymph nodes in different regions of the body](#) ☆
- [Preliminary results for characterization of pelvic lymph nodes in patients with prostate cancer by diffusion-weighted MR-imaging.](#)
- [Whole-body diffusion-weighted imaging with apparent diffusion coefficient mapping for treatment response assessment in patients with diffuse large B-cell lymphoma: pilot study.](#)
- [Application of whole body diffusion weighted mr imaging for diagnosis and staging of malignant lymphoma](#)
- [Evaluation of Diffusion-Weighted MRI for Pretherapeutic Assessment and Staging of Lymphoma: Results of a Prospective Study in 140 Patients](#)

Share this paper:    

View more about this paper here: <https://typeset.io/papers/improving-lymph-node-characterization-in-staging-malignant-1c49fffafo>

1 **ABSTRACT**

2 **Background:** Correct staging and treatment initiation in malignant lymphoma depends on
3 accurate lymph node characterization. However, nodal assessment based on conventional and
4 diffusion-weighted (DWI) magnetic resonance imaging, remains challenging, particularly in
5 smaller nodes.

6 **Purpose:** To evaluate first order apparent diffusion coefficient (ADC) texture parameters
7 compared to mean ADC for lymph node characterization in Non-Hodgkin lymphoma (NHL)
8 using whole-body DWI (WB-DWI).

9 **Study type:** Retrospective

10 **Population:** 28 patients with NHL

11 **Field strength/sequence:** 3 Tesla whole-body DWI using 2 b-values (0-1000 s/mm²)

12 **Assessment:** Regions of interest were drawn on the 3 most hyperintense lymph nodes on
13 b1000-images, irrespective of size, in all nodal body regions. Diagnostic performance of mean
14 ADC (ADC_{mean}) was compared with first order ADC texture parameters: standard deviation
15 (ADC_{stdev}), kurtosis (ADC_{kurt}) and skewness (ADC_{skew}). Additional subanalyses focused on
16 accuracy of ADC_{mean} and ADC texture parameters in different lymph node volumes and nodal
17 regions.

18 **Statistical tests:** Benign and malignant nodes were compared using Mann-Whitney-U-tests
19 with FDG-PET/CT and bone marrow biopsy as reference standard. Receiver-Operating-
20 Characteristic analyses were performed to determine cut-off values and calculate sensitivity,
21 specificity, accuracy, positive and negative predictive value (PPV, NPV).

22 **Results:** ADC_{mean} (p=0.008), ADC_{skew} and ADC_{kurt} differed significantly between benign and
23 malignant nodes (p<0.001), while ADC_{stdev} didn't (p=0.21). ADC_{skew} was the best
24 discriminating parameter with 79% sensitivity, 86% specificity, 83% accuracy, 85% PPV and

25 81% NPV. In every volume category, ADC_{skew} yielded the highest accuracy (88% in 0-25th
26 percentile volume, 75% in 25th-75th percentile, 93% in 75-100th percentile). On a per-region
27 basis, ADC_{skew} accuracy varied 13.6% between nodal regions, while ADC_{mean} , ADC_{kurt} and
28 ADC_{stdev} showed interregional variation of 17.4%, 20.3% and 14.9%, respectively.

29 **Data conclusion:** First order ADC texture analysis with WB-DWI improved lymph node
30 characterization compared to ADC_{mean} . ADC_{skew} was the most accurate and robust
31 discriminatory parameter over all lymph node volumes and nodal body regions.

32

33 **Keywords:** apparent diffusion coefficient, diffusion-weighted, MR imaging, lymphoma,
34 staging

35 INTRODUCTION

36 Non-Hodgkin lymphoma (NHL) can arise virtually anywhere in the body, primarily in nodal
37 tissue, and typically disseminates systemically via the lymphatics. Therefore, a whole-body
38 imaging technique is required in order to cover all potentially affected regions. Currently,
39 hybrid 18-Fluoro-deoxyglucose positron emission tomography computed tomography (18-
40 FDG-PET/CT) is accepted as the imaging method of choice to stage aggressive NHL and
41 FDG-avid indolent lymphoma¹. However, FDG-PET/CT is cost-intensive, not always widely
42 available, and is associated with a substantial amount of ionizing radiation.

43 Whole-body diffusion-weighted magnetic resonance imaging (WB-DWI) might serve as an
44 alternative radiation-free imaging technique for lymphoma staging purposes²⁻¹². Affected
45 sites usually present as easily detectable masses, which are commonly hyperintense on the
46 diffusion-weighted images acquired using a b-value of 1000 s/mm² (b1000-images) and
47 hypointense on the calculated apparent coefficient diffusion (ADC) maps. However, smaller –
48 even normal sized - nodes can also harbor malignant deposits and these might be difficult to
49 identify as lymph nodes inherently exhibit high signal on b1000-images and low ADC
50 values¹³. Furthermore, considerable ADC overlap exists between reactive and malignant
51 lymph nodes, decreasing the technique's specificity¹⁴.

52 First order texture analysis^{15,16} is an emerging tool in MRI analysis, consisting of the
53 determination of histogram derived parameters, which may provide insight on tumor
54 heterogeneity. This approach has proven useful for differentiating between tumor types and
55 histological grades¹⁷⁻²⁷ or assessing treatment response²⁸⁻³⁰. To date, texture analysis to
56 discriminate benign and affected nodes has not been reported in malignant lymphoma.

57 Therefore, the aim of this study was to evaluate first order ADC texture parameters compared
58 to the more commonly used mean ADC for lymph node characterization in NHL with WB-
59 DWI with FDG-PET/CT as the reference of standard.

60 MATERIALS AND METHODS

61 *Patients*

62 This study was approved by the local ethics committee and all patients gave written informed
63 consent prior to inclusion. Inclusion criteria were a (1) new diagnosis, of (2) histopathological
64 proven (3) aggressive or indolent lymphoma. Exclusion criteria were defined as (1) general
65 contraindications to MRI (e.g. pacemaker, claustrophobia) and (2) treatment initiation prior to
66 the WB-DWI or between WB-DWI and FDG-PET/CT scans.

67 Twenty-eight patients (20 men and 8 women; age range 29-81 years, mean 60 years) with a
68 new diagnosis of NHL (20 diffuse large B-cell lymphoma (DLBCL), 2 T-cell lymphoma
69 (TCL) and 6 follicular lymphoma (FL)) were consecutively included. Patient characteristics
70 are summarized in Table 1. Histopathological diagnosis and determination of subtypes were
71 done according to the criteria of the current WHO classification of hematological and
72 lymphoid malignancies³¹ by an experienced pathologist.

73 All patients underwent WB-DWI in addition to routine clinical diagnostic procedures
74 including physical examination, blood analysis, histological lymph node examination, bone
75 marrow biopsy and FDG-PET/CT.

76 Chemotherapy is the standard treatment, although exact regimens vary between tumor types.
77 Most common regimens in aggressive lymphoma are based on CHOP [cyclophosphamide,
78 hydroxydaunorubicin (doxorubicin), vincristine, and prednisone/prednisolone] with or
79 without Rituximab [R]; treatment of indolent lymphoma is generally based on CVP
80 [cyclophosphamide, vincristine, and prednisone].

81

82

83

84 ***Imaging Techniques***

85 *WB-DWI*

86 Whole-body imaging covering the brain down to the proximal 1/3rd of the upper legs was
87 performed on a 3 Tesla (T) MRI system (Ingenia; Philips, Best, The Netherlands),
88 with parallel radiofrequency transmission and phased-array head-neck, body and spine coils.
89 Free-breathing short inversion time (TI) inversion recovery STIR WB-DWI was acquired in
90 the transverse plane in 4 consecutive imaging stations (head/ neck, chest, upper abdomen and
91 pelvis). Each imaging station consisted of 50 slices, 5 mm slice thickness, intersection gap of
92 0.1 mm, field of view (FoV) of 420 x 329 mm, voxel resolution of 4.6 x 4.7 x 5 mm,
93 repetition time (TR)/TI of 8454/250 ms and echo time (TE) of 67 ms, with b-values of 0 (b0)
94 and 1000 s/mm² (b1000). Total sequence time was 15 minutes and 21 seconds. For
95 interpretation, coronal 5-mm thick whole-body multiplanar reconstruction (MPR) images
96 were generated by the scanner software from the b0, and b1000 images as well as from the
97 ADC-maps. For anatomical reference, whole-body STIR fat-suppressed T2-weighted
98 turbospin echo (TSE) images were acquired in the coronal plane in 3 consecutive imaging
99 stations. Each station consisted of 40 slices; 6 mm slice thickness, intersection gap of 0.6 mm,
100 FoV of 263 mm x 228-452 mm, voxel resolution of 1.5 x 1.7 x 6 mm and TR/ TI of 2324-
101 9294/200 ms and TE of 80 ms. Total sequence time was 6 minutes and 8 seconds. Finally, a
102 sagittal T1-weighted TSE sequence was acquired over the spine in 2 consecutive stations
103 (thoracic and lumbar spine) with the following parameters: 15 slices per station, 4 mm slice
104 thickness, intersection gap of 0.4 mm, FoV 260 x 380 mm, voxel resolution of 1.3 x 1 x 4 mm
105 and TR/TE of 378/7 ms. Total sequence time was 4 min and 24 s.

106

107

108 *FDG-PET/CT*

109 Patients fasted for 6 hours prior to the integrated FDG-PET/CT examination (Biograph 40
110 TruePoint with TrueV, Siemens Medical Solutions, Erlangen, Germany). FDG-PET-images
111 were acquired 60 minutes after intravenous administration of FDG at an average dose of 302.6
112 MBq (range: 220-388 MBq) and in the same session a single-section, whole-body, spiral CT
113 (40-slice Siemens Sensation, 85 mAs, 120 kV, slice thickness 5 mm, collimation 24 x 1.2 mm,
114 table feed 23 mm/rotation) was performed after intravenous injection of 120 ml of a contrast
115 agent containing 300 mg iodine/ml.

116

117

118 *Image Analysis*

119 *Whole-body DWI*

120 Two radiologists, (a board-certified radiologist with 10 years of experience (VV) and senior
121 resident (KDP), blinded to all other study and clinical data analyzed the DW images in
122 consensus using semi-automated contouring software (in-house developed MeVisLab (MeVis
123 Medical Solutions AG, Bremen, Germany) program enabling tissue segmentation based on
124 region growing). Lymph node regions were subdivided as follows: cervical (left/right),
125 axillary (left/right), mediastinal and hilar, mesenteric, retroperitoneal (left/right), iliac
126 (left/right) and inguinal (left/right). Lymph nodes were localized on the b1000 images. As
127 small nodes can also have lymphomatous involvement, we chose not to use size criteria, but
128 selected nodes based on their b1000 signal intensity (SI). Per region - both left and right when
129 applicable - three lymph nodes appearing most hyperintense at b1000 images were selected
130 for quantitative analysis. Each lymph node was consecutively annotated with the cursor and
131 automatically contoured by the software, to form a 3-dimensional ROI per lymph node. In

132 case of mismatch between the ROI and nodal contour, the ROI contour was manually adapted
133 to fit the nodal contour. ROIs were placed over the entire lymph node and in case of obvious
134 solid and necrotic tissue on b1000 images ROIs were placed over the solid tissue portions.
135 From these ROIs, pixel-wise ADC values were extracted for construction of an ADC
136 histogram for each delineated lymph node, from which the mean (ADC_{mean}), standard
137 deviation (ADC_{stdev}), kurtosis (ADC_{kurt}) and skewness (ADC_{skew}) were calculated.

138

139 *Reference Standard Of Treatment Outcome*

140 The histologic confirmation of the presence of lymphoma remains the reference standard.
141 Routinely, a definite diagnosis of malignant lymphoma is made based on histopathological
142 analysis of an excisional biopsy of an accessible node. However, as biopsy of every suspected
143 lesion is practically and ethically not feasible, instead we used FDG-PET/CT, which was
144 evaluated using the same nodal regional distribution as for WB-MRI/DWI, as an imperfect
145 standard of reference to characterize the remainder of the lymph node regions. PET was
146 performed as part of standard clinical care and reported by a nuclear medicine physician with
147 10 years of experience and a special interest in lymphoma, not blinded for clinical or other
148 imaging data. A lymph node was considered PET-positive for lymphoma when FDG-uptake,
149 marked higher than the background, was present in a location incompatible with normal
150 anatomy or physiology. In case of discrepancies, follow-up imaging was used to characterize
151 conspicuous lesions. Any lesion that decreased in volume during treatment was designated as
152 malignant.

153

154

155 *Statistical analysis*

156 Statistical analysis was done with SPSS 13.0 for Windows (SPSS, Chicago, IL, US). A P-
157 value < 0.05 was considered statistically significant.

158 Delineated lymph nodes on WB-DWI were correlated to FDG-PET/CT on a per-lymph node
159 basis after all image interpretation was concluded. Descriptive values were calculated for
160 every ADC parameter and ANOVA test with patient ID as random effect were conducted to
161 check for significant differences between malignant and benign lymph nodes. ANOVA tests
162 with Bonferroni correction were performed to investigate the possible confounding effect of
163 factors such as disease stage, lymphoma subtype and lymph node volume on the ADC value.
164 Next, Receiver-Operating-Characteristic (ROC) curves were constructed from which an
165 optimal threshold equally weighting sensitivity and specificity for malignant lymph node
166 detection was calculated. Subsequently, sensitivity, specificity, accuracy, negative and
167 positive predictive value (NPV and PPV) were determined.

168 Additionally, the potential influence of nodal volume on parameter accuracy was investigated.
169 For this purpose, lymph nodes were divided in 3 volume categories: the 25th percentile
170 smallest nodes ($\leq p_{25}$), the 25th percentile largest nodes ($\geq p_{75}$) and all lymph nodes with a
171 volume in between (p_{25} - p_{75}). Also, the potential influence of nodal body region on parameter
172 accuracy was explored. As such, per-parameter Mann-Whitney U tests and ROC curve
173 construction were repeated for every lymph node volume category and for the separate lymph
174 node regions and associated accuracies were calculated.

175

176

177

178 **RESULTS**

179 *First Order ADC Texture Parameters*

180 All ADC histogram derived parameters demonstrated a significant difference between benign
181 (n=140) and malignant nodes (n=101) (ADC_{mean} : $F= 8.33$, $p=0.008$; ADC_{skew} : $F= 44.85$,
182 $p<0.001$; ADC_{kurt} : $F= 15.15$, $p<0.001$), except for ADC_{stdev} ($F= 1.63$, $p= 0.21$). ADC_{skew}
183 yielded the highest AUC of 0.85 (Figure 1), attaining higher accuracy than the other first
184 order ADC texture parameters, with a higher specificity of 86.4% and higher sensitivity of
185 79.2% (Table 2). A patient-by-patient analysis didn't reveal significant influence on any of
186 the ADC values (ADC_{mean} : $F= 0.55$, $p= 0.93$; ADC_{skew} : $F= 1.05$, $p= 0.46$; ADC_{kurt} : $F= 1.07$,
187 $p= 0.46$). In addition, as demonstrated by post hoc correction, ADC values were not impacted
188 by variations in stage (ADC_{mean} : $F= 0.17$, $p= 0.84$; ADC_{skew} : $F= 0.81$, $p= 0.45$; ADC_{kurt} : $F=$
189 1.91 , $p= 0.13$), lymphoma subtype (ADC_{mean} : $F= 0.91$, $p=0.34$; ADC_{skew} : $F= 1.81$, $p= 0.18$;
190 ADC_{kurt} : $F= 0.083$, $p=0.77$) or nodal volume (ADC_{mean} : $F= 1.46$, $p=0.07$; ADC_{skew} : $F= 0.93$,
191 $p= 0.64$; ADC_{kurt} : $F= 1.14$, $p= 0.31$). Nodal region had a significant effect on ADC_{mean} ($F=$
192 7.70 , $p<0.001$), but not on ADC_{kurt} ($F= 2.15$, $p=0.049$) or ADC_{skew} ($F= 1.42$, $p=0.21$).

193

194 ADC_{mean} attained poor sensitivity of 58.4%, resulting in decreased NPV and accuracy.
195 Inversely to ADC_{mean} , ADC_{kurt} demonstrated a higher sensitivity, but lower specificity with
196 comparable accuracies of 65.8% and 67.2% for ADC_{kurt} and ADC_{mean} , respectively.
197 Malignant nodes expressed lower ADC_{mean} (1.16 vs $1.43 \cdot 10^{-3}$ mm²/s), higher ADC_{kurt} (4.12
198 vs 3.22) and higher ADC_{skew} values (0.79 vs -0.002) than benign nodes (Figure 2).

199

200

201 ***First Order ADC Texture Parameter Analysis And Lymph Node Volume***

202 Accuracy of ADC parameters in relation to lymph node volume is shown in Table 3. For all
203 volume categories, ADC_{skew} was the best discriminating parameter. In the $\leq p25$ nodes
204 (median volume [range] = 0.51 [0.10-0.65] cm^3), ADC_{skew} accuracy was 88.3%, which was
205 11%, 21% and 30% higher than the accuracies attained for ADC_{mean} , ADC_{kurt} and ADC_{stdev} ,
206 respectively. In the p25-p75 nodes (1.60 [0.66-3.69] cm^3), ADC_{skew} was the only significant
207 parameter with an accuracy of 75.2%, 23-25% higher than the accuracy of the remainder of
208 the first order texture parameters. In the $\geq p75$ nodes (62.97 [3.70-287.46] cm^3), all parameters
209 except ADC_{mean} reached statistical significance with an ADC_{mean} accuracy of 68.3%, while
210 the other parameters showed higher accuracies between 81.7-93.3%, the highest of which was
211 again attained by ADC_{skew} .

212

213 ***First Order ADC Texture Parameter Analysis And Lymph Node Region***

214 Using a per nodal region cut-off improved accuracy of ADC_{mean} and ADC texture parameters
215 in the majority of lymph node regions, but also revealed interregional variations (Table 4).
216 ADC_{skew} was the most robust parameter with an accuracy ranging between 78.1% and 91.4%
217 (= total accuracy range of 13.3%) between lymph node regions. In relation to the overall
218 accuracy, the use of a regional cut-off resulted in a 5.4% accuracy decrease for mesenteric and
219 mediastinal nodes while the accuracy increased with 8% for inguinal nodes. ADC_{mean}
220 variation of accuracy between regions was 17.4% with an accuracy increase of 4.2% in the
221 iliac and 16.1% in the axillary nodes relative to the overall accuracy. ADC_{kurt} and ADC_{stdev}
222 demonstrated an interregional accuracy variation of 20.3% and 14.9%, respectively. For both
223 parameters, a regional cut-off resulted in higher accuracies in all lymph node regions of up to
224 23.3% for ADC_{kurt} in the mesenteric nodes and 15.4% for ADC_{stdev} in the inguinal nodes.

225 As indicated by the regional cut-off values, nodes in certain lymph node regions exhibited
226 lower or higher ADC_{mean} and texture parameter values (Table 4, Figure 3). For ADC_{mean} ,
227 mediastinal and retroperitoneal nodes attained higher values in comparison with the other
228 regions, especially compared to the axillary lymph nodes, which attained the lowest ADC_{mean}
229 value. ADC_{skew} was lower in the mediastinal lymph node and higher in the iliac and inguinal
230 region. Similarly, mediastinal and mesenteric nodes exhibited lower ADC_{kurt} values, while
231 axillary and iliac nodes demonstrated a high ADC_{kurt} . Conversely, the highest ADC_{stdev} values
232 were found for mediastinal and mesenteric nodes, and the lowest for inguinal nodes.

233

234 **DISCUSSION**

235 This study demonstrated that first order ADC texture analysis may improve lymph node
236 characterization in malignant lymphoma compared to the use of ADC_{mean} - a commonly used,
237 but unvalidated quantitative measure in lymphoma. ADC_{skew} proved to be the most accurate
238 parameter to differentiate benign from lymphomatous nodes, and the most robust one in terms
239 of lymph node size and lymph node region.

240 Quantitative DWI analysis of nodes has been mostly investigated in the context of
241 differentiating metastatic, lymphomatous and benign cervical lymphadenopathy³²⁻³⁸, and
242 consisted of ADC_{mean} calculations with reported values of nodes involved with lymphoma
243 ranging from $0.223 \pm 0.056 \times 10^{-3} \text{ mm}^2/\text{s}$ to $0.97 \pm 0.27 \times 10^{-3} \text{ mm}^2/\text{s}$. The ADC_{mean} values
244 demonstrated in lymphoma staging studies using a whole-body protocol^{10,39,40} were within
245 this range ($0.70 \pm 0.16 \times 10^{-3} \text{ mm}^2/\text{s}$ to $0.87 \pm 0.17 \times 10^{-3} \text{ mm}^2/\text{s}$). In this study, a slightly
246 higher ADC_{mean} of $1.09 \pm 0.28 \times 10^{-3} \text{ mm}^2/\text{s}$ for malignant nodes was found, which might be
247 explained by some methodological differences. In the aforementioned studies, ROIs were

248 manually drawn on calculated ADC maps, while in the current study a semi-automated
249 delineation tool was used and ROIs were drawn on native DWI images. Also, the use of a
250 scanner with different field strength – 3T study in the current study, and 1.5 T in previous
251 literature -, may have resulted in absolute ADC value differences.

252 Using a ADC_{mean} cut-off value of $0.80 \times 10^{-3} \text{ mm}^2/\text{s}$, Kwee et al.⁴¹ yielded a sensitivity and
253 specificity of 78% and 100% to detect lymphomatous nodes. Conversely, we found ADC_{mean}
254 sensitivity of only 58.4% due to great overlap in ADC_{mean} values between benign and
255 malignant nodes. Instead, first order texture analysis performed in this study demonstrated
256 ADC_{skew} to be the parameter attaining highest sensitivity of 79.2% and specificity of 86.4%.
257 This is in line with previous studies in other tumor types, showing the potential of this type of
258 analysis for the discrimination of benign and malignant lesions. For instance, a significantly
259 higher ADC_{skew} and lower ADC_{mean} were found in malignant endometrial⁴² and breast
260 lesions⁴³, while a study by Suo et al. concerning bladder lesions⁴⁴ showed ADC_{skew} , ADC_{kurt}
261 and ADC_{mean} to differ significantly between benign bladder lesions and bladder carcinoma.
262 Only the group of Wang et al.⁴⁵ has applied first order ADC texture analysis in malignant
263 lymphoma to differentiate lymphoma from metastatic nodes in the head and neck region, but
264 to our knowledge no other literature is available on first order texture analysis of lymphoma
265 nodes using a whole body protocol.

266 The majority of studies using a quantitative analysis of WB-DWI to stage malignant
267 lymphoma included enlarged nodes^{4,6,10,40} only with a diameter of more than 10 mm.
268 However, as normal sized nodes may contain malignancy as well, no size cut-off was
269 implemented in our study. A subgroup analysis evaluating the diagnostic performance of
270 ADC_{mean} and ADC texture parameters in different nodal volume categories demonstrated that
271 ADC_{skew} was the most accurate parameter. In all volume categories ADC_{mean} attained rather

272 low accuracies ranging from 55% to 77%. In contrast to ADC_{skew} , the discriminatory
273 capability of the remainder of the ADC texture parameters in middle-sized and small nodes
274 was limited, although their attained accuracy in large nodes and nodal masses was good to
275 excellent.

276 Besides accuracy variations in relation to nodal volume, variations were also noticed between
277 lymph node regions. The use of regional cut-off values resulted in an increase of the
278 diagnostic performance. Previous studies used an overall cut-off value based on either their
279 own data^{2,10,39,40} without the performance of a regional subgroup analysis or based on data
280 from the literature⁴¹, although these are mainly based on studies performed in cervical and/or
281 pelvic nodes only. Yet, mediastinal and retroperitoneal nodes exhibited higher ADC_{mean}
282 values than other nodal regions, which might be due to a variety of factors such as partial
283 volume effect, motion artefacts (bowel, respiration) and distance to the coil. Although this has
284 not been addressed before, it is of importance to avoid false negative and positive results
285 when assessing individual nodal regions, and raises the question whether a regional cut-off
286 should be used instead of an overall cut-off. The accuracy increase would probably be more
287 noted for ADC_{mean} , a quite variable parameter in this study, than for a more robust parameter
288 like ADC_{skew} .

289 This study had several limitations. First, quantitative parameters were used, the value of
290 which is dependent of a multitude of factors (field strength, MRI scanner hard- and software,
291 delineation, post-processing, etc.) and therefore prone for variations between observers and
292 centers. In addition, the delineation of small nodes results in histograms with a small number
293 of pixels, hence, small changes might induce large variations in measurements. We tried to
294 overcome these limitations by applying a semi-quantitative delineation method, allowing for
295 observer dependent node and ROI size selection, yet with automatic ROI delineation and

296 parameter calculations. This method also counteracts – at least partially- another important
297 hurdle of quantitative analysis, being time-efficacy, which is currently limiting its
298 implementation in daily practice. Furthermore, as lymphoma primarily present with large
299 masses easily detected by visual WB-DWI analysis, a further reduction in analysis time might
300 be achieved by performing quantitative analysis of equivocal nodes only. Finally, multiple
301 confounding factors such as disease stage and lymphoma subtype as well as patient clustering
302 may have affected our results. We tried to identify these factors by including corrections for
303 multiple comparisons in the analysis. Yet, the small population is an important limiting factor,
304 which might have hindered a meaningful statistical analysis. Nevertheless, our results were
305 highly significant, warranting larger-scale studies to validate our findings. These larger
306 datasets would not only allow for a more accurate evaluation of confounding effects, but
307 should also explore the inter- and intra-observer variability. Of note, owing to the potential
308 effect of data clustering in this limited dataset, the present optimal cut-offs and accuracies
309 might differ from those found in larger studies.

310 In conclusion, first order ADC texture analysis using WB-DWI may improve lymph node
311 characterization in malignant lymphoma. ADC_{mean} , although commonly used, demonstrated
312 low accuracy, in contrast to ADC_{skew} , which proved to be the best parameter to characterize
313 lymph nodes regardless of lymph node volume or nodal body region.

314

315

REFERENCES

1. Barrington SF, Mikhaeel NG, Kostakoglu L, et al. Role of imaging in the staging and response assessment of lymphoma: consensus of the International Conference on Malignant Lymphomas Imaging Working Group. *J Clin Oncol*. 2014;32(27):3048-3058.
2. Mayerhoefer ME, Karanikas G, Kletter K, et al. Evaluation of diffusion-weighted MRI for pretherapeutic assessment and staging of lymphoma: results of a prospective study in 140 patients. *Clin Cancer Res*. 2014;20(11):2984-2993.
3. Littooij AS, Kwee TC, Barber I, et al. Whole-body MRI for initial staging of paediatric lymphoma: prospective comparison to an FDG-PET/CT-based reference standard. *Eur Radiol*. 2014;24(5):1153-1165.
4. Stéphane V, Samuel B, Vincent D, et al. Comparison of PET-CT and magnetic resonance diffusion weighted imaging with body suppression (DWIBS) for initial staging of malignant lymphomas. *Eur J Radiol*. 2013;82(11):2011-2017.
5. Lin C, Luciani A, Itti E, et al. Whole-body diffusion magnetic resonance imaging in the assessment of lymphoma. *Cancer Imaging*. 2012;12:403-408.
6. Gu J, Chan T, Zhang J, Leung AYH, Kwong Y-L, Khong P-L. Whole-body diffusion-weighted imaging: the added value to whole-body MRI at initial diagnosis of lymphoma. *AJR Am J Roentgenol*. 2011;197(3):W384-91.
7. Abdulqadhr G, Molin D, Aström G, et al. Whole-body diffusion-weighted imaging compared with FDG-PET/CT in staging of lymphoma patients. *Acta Radiol*. 2011;52(2):173-180.
8. Kwee TC, Takahara T, Vermoolen MA, Bierings MB, Mali WP, Nievelstein RAJ. Whole-body diffusion-weighted imaging for staging malignant lymphoma in children. *Pediatr Radiol*. 2010;40(10):1592-602-1.
9. Kwee TC, Vermoolen MA, Akkerman EA, et al. Whole-body MRI, including diffusion-weighted imaging, for staging lymphoma: comparison with CT in a prospective multicenter study. *J Magn Reson Imaging*. 2014;40(1):26-36.
10. Li S, Xue H-D, Li J, et al. Application of whole body diffusion weighted MR imaging for diagnosis and staging of malignant lymphoma. *Chin Med Sci J*. 2008;23(3):138-144.
11. Balbo-Mussetto A, Cirillo S, Bruna R, et al. Whole-body MRI with diffusion-weighted imaging: a valuable alternative to contrast-enhanced CT for initial staging of aggressive lymphoma. 2016;71(3).
12. Albano D, Patti C, La Grutta L, et al. Comparison between whole-body MRI with diffusion-weighted imaging and PET/CT in staging newly diagnosed FDG-avid lymphomas. 2016;85(2).
13. Kwee TC, Takahara T, Luijten PR, Nievelstein R a J. ADC measurements of lymph nodes: inter- and intra-observer reproducibility study and an overview of the literature. 2010;75(2):215-220.
14. Chawla S, Kim S, Wang S, Poptani H. Diffusion-weighted imaging in head and neck cancers. *Future Oncol*. 2009;5(7):959-975.
15. Davnall F, Yip CSP, Ljungqvist G, et al. Assessment of tumor heterogeneity: an

- emerging imaging tool for clinical practice? *Insights Imaging*. 2012;3(6):573-589.
16. Just N. Improving tumour heterogeneity MRI assessment with histograms. *Br J Cancer*. 2014;111(12):2205-2213.
 17. Downey K, Riches SF, Morgan VA, et al. Relationship between imaging biomarkers of stage I cervical cancer and poor-prognosis histologic features: quantitative histogram analysis of diffusion-weighted MR images. *AJR Am J Roentgenol*. 2013;200(2):314-320.
 18. Woo S, Cho JY, Kim SY, Kim SH. Histogram analysis of apparent diffusion coefficient map of diffusion-weighted MRI in endometrial cancer: a preliminary correlation study with histological grade. *Acta radiol*. 2014;55(10):1270-1277.
 19. Ahn SJ, Choi SH, Kim Y-J, et al. Histogram analysis of apparent diffusion coefficient map of standard and high B-value diffusion MR imaging in head and neck squamous cell carcinoma: a correlation study with histological grade. *Acad Radiol*. 2012;19(10):1233-1240.
 20. Pereira JAS, Rosado E, Bali M, Metens T, Chao S-L. Pancreatic neuroendocrine tumors: correlation between histogram analysis of apparent diffusion coefficient maps and tumor grade. *Abdom Imaging*. 2015;40(8):3122-3128.
 21. Kim EJ, Kim SH, Park GE, et al. Histogram analysis of apparent diffusion coefficient at 3.0t: Correlation with prognostic factors and subtypes of invasive ductal carcinoma. *J Magn Reson Imaging*. 2015;42(6):1666-1678.
 22. Takahashi M, Kozawa E, Tanisaka M, Hasegawa K, Yasuda M, Sakai F. Utility of histogram analysis of apparent diffusion coefficient maps obtained using 3.0T MRI for distinguishing uterine carcinosarcoma from endometrial carcinoma. *J Magn Reson Imaging*. 2016;43(6):1301-1307.
 23. Lin Y, Li H, Chen Z, et al. Correlation of histogram analysis of apparent diffusion coefficient with uterine cervical pathologic finding. *AJR Am J Roentgenol*. 2015;204(5):1125-1131.
 24. Brynolfsson P, Nilsson D, Henriksson R, et al. ADC texture--an imaging biomarker for high-grade glioma? *Med Phys*. 2014;41(10):101903.
 25. Ryu YJ, Choi SH, Park SJ, Yun TJ, Kim J-H, Sohn C-H. Glioma: application of whole-tumor texture analysis of diffusion-weighted imaging for the evaluation of tumor heterogeneity. Hess CP, ed. *PLoS One*. 2014;9(9):e108335.
 26. Rozenberg R, Thornhill RE, Flood TA, Hakim SW, Lim C, Schieda N. Whole-Tumor Quantitative Apparent Diffusion Coefficient Histogram and Texture Analysis to Predict Gleason Score Upgrading in Intermediate-Risk 3 + 4 = 7 Prostate Cancer. *AJR Am J Roentgenol*. 2016;206(4):775-782.
 27. Hao Y, Pan C, Chen W, Li T, Zhu W, Qi J. Differentiation between malignant and benign thyroid nodules and stratification of papillary thyroid cancer with aggressive histological features: Whole-lesion diffusion-weighted imaging histogram analysis. *J Magn Reson Imaging*. 2016;44(6):1546-1555.
 28. Liang H-Y, Huang Y-Q, Yang Z-X, Ying-Ding, Zeng M-S, Rao S-X. Potential of MR histogram analyses for prediction of response to chemotherapy in patients with colorectal hepatic metastases. *Eur Radiol*. 2016;26(7):2009-2018.
 29. Kyriazi S, Collins DJ, Messiou C, et al. Metastatic ovarian and primary peritoneal

- cancer: assessing chemotherapy response with diffusion-weighted MR imaging--value of histogram analysis of apparent diffusion coefficients. *Radiology*. 2011;261(1):182-192.
30. Breit A, Heuck A, Lukas P, Kneschaurek P, Mayr M. Tumor Response Monitoring and Treatment Planning: Advanced Radiation Therapy. 2013.
 31. Swerdlow SH, Campo E, Pileri SA, et al. The 2016 revision of the World Health Organization classification of lymphoid neoplasms. *Blood*. 2016;127(20).
 32. Fong D, Bhatia KSS, Yeung D, King AD. Diagnostic accuracy of diffusion-weighted MR imaging for nasopharyngeal carcinoma, head and neck lymphoma and squamous cell carcinoma at the primary site. *Oral Oncol*. 2010;46(8):603-606.
 33. Sumi M, Van Cauteren M, Nakamura T. MR microimaging of benign and malignant nodes in the neck. *AJR Am J Roentgenol*. 2006;186(3):749-757.
 34. Maeda M, Kato H, Sakuma H, Maier SE, Takeda K. Usefulness of the Apparent Diffusion Coefficient in Line Scan Diffusion-Weighted Imaging for Distinguishing between Squamous Cell Carcinomas and Malignant Lymphomas of the Head and Neck. *Am J Neuroradiol*. 2005;26(5).
 35. Sumi M, Sakihama N, Sumi T, et al. Discrimination of metastatic cervical lymph nodes with diffusion-weighted MR imaging in patients with head and neck cancer. *AJNR Am J Neuroradiol*. 2003;24(8):1627-1634.
 36. Holzapfel K, Duetsch S, Fauser C, Eiber M, Rummeny EJ, Gaa J. Value of diffusion-weighted MR imaging in the differentiation between benign and malignant cervical lymph nodes. *Eur J Radiol*. 2009;72(3):381-387.
 37. King AD, Ahuja AT, Yeung DKW, et al. Malignant Cervical Lymphadenopathy: Diagnostic Accuracy of Diffusion-weighted MR Imaging. *Radiology*. 2007;245(3):806-813.
 38. Abdel Razek AAK, Soliman NY, Elkhamary S, Alsharaway MK, Tawfik A. Role of diffusion-weighted MR imaging in cervical lymphadenopathy. *Eur Radiol*. 2006;16(7):1468-1477.
 39. Wu X, Pertovaara H, Dastidar P, et al. ADC measurements in diffuse large B-cell lymphoma and follicular lymphoma: a DWI and cellularity study. *Eur J Radiol*. 2013;82(4):e158-64.
 40. Lin C, Luciani A, Itti E, et al. Whole-body diffusion-weighted magnetic resonance imaging with apparent diffusion coefficient mapping for staging patients with diffuse large B-cell lymphoma. *Eur Radiol*. 2010;20(8):2027-2038.
 41. Kwee TC, Ludwig I, Uiterwaal CS, et al. ADC measurements in the evaluation of lymph nodes in patients with non-Hodgkin lymphoma: feasibility study. *Magn Reson Mater Physics, Biol Med*. 2011;24(1):1-8.
 42. Kierans AS, Doshi AM, Dunst D, Popiolek D, Blank S V., Rosenkrantz AB. Retrospective Assessment of Histogram-Based Diffusion Metrics for Differentiating Benign and Malignant Endometrial Lesions. *J Comput Assist Tomogr*. 2016;40(5):723-729.
 43. Suo S, Zhang K, Cao M, et al. Characterization of breast masses as benign or malignant at 3.0T MRI with whole-lesion histogram analysis of the apparent diffusion coefficient. *J Magn Reson Imaging*. 2016;43(4):894-902.

44. Suo S-T, Chen X-X, Fan Y, et al. Histogram analysis of apparent diffusion coefficient at 3.0 T in urinary bladder lesions: correlation with pathologic findings. *Acad Radiol.* 2014;21(8):1027-1034.
45. Wang Y-J, Xu X-Q, Hu H, et al. Histogram analysis of apparent diffusion coefficient maps for the differentiation between lymphoma and metastatic lymph nodes of squamous cell carcinoma in head and neck region. *Acta radiol.* September 2017:28418511773068.

TABLES

Table 1. Patient characteristics

	Aggressive NHL n=22	Indolent NHL n=6
Mean age (range) y	59 (17-83)	85 (48-75)
Sex		
<i>Male</i>	16 (72.7%)	4 (66.7%)
<i>Female</i>	6 (27.3%)	2 (33.3%)
Stage		
<i>I</i>	3 (13.6%)	1 (16.7%)
<i>II</i>	8 (36.4%)	0
<i>III</i>	4 (18.2%)	3 (16.7%)
<i>IV</i>	7 (31.8%)	4 (66.7%)
Subtype		
<i>Grade 1-2</i>		5 (83.3%)
<i>Grade 3a</i>		1 (16.7%)
<i>DLBCL</i>	17 (77.3%)	
<i>Burkitt</i>	2 (9.1%)	
<i>Primary mediastinal BCL</i>	1 (4.5%)	
<i>Peripheral TCL</i>	2 (9.1%)	

DLBCL= diffuse B-cell lymphoma; BCL= B-cell lymphoma;
TCL= T-cell lymphoma

Table 2. Cut-off value and corresponding sensitivity, specificity, accuracy, negative predictive value and positive predictive value for mean ADC and ADC texture parameters

ADC				
	Mean ($\times 10^{-3}$ mm ² /s)	Skewness	Kurtosis	Stdev ($\times 10^{-3}$ mm ² /s)
Cut-off	1.11	0.38	2.95	.22
Median [range] Ben (n=140)	1.34[.73-2.67]	.06[-1.61-1.45]	2.79[1.54-11.96]	.19[.03-.85]
Median [range] Mal (n=101)	1.04[.63-3.22]	.74[-1.14-2.05]	3.59[1.94-9.69]	.23[.03-.52]
Sensitivity (%)	58.4	79.2	76.2	55.4
Specificity (%)	73.6	86.4	57.9	61.4
Accuracy (%)	67.2	83.4	65.6	58.9
NPV (%)	71.0	85.2	77.1	65.7
PPV (%)	61.5	80.8	56.6	50.9

Ben= benign; Mal= malignant; Stdev= standard deviation;
NPV= negative predictive value; PPV= positive predictive value

Table 3. Accuracy of the ADC mean and texture parameters in volume-based subgroups

	<P25 (n=60)			P25-75 (n=121)			>P75 (n=60)					
	mean [range] volume =			mean [range] volume =			mean [range] volume =					
	0.51 [0.10-0.65] cm³			1.60 cm³[0.66-3.69] cm³			62.97 [3.70-287.46] cm³					
	Acc (%)	Median [range]		p-value	Acc (%)	Median [range]		p-value	Acc (%)	Median [range]		p-value
		Ben (n=54)	Mal (n=6)			Ben (n=80)	Mal (n=41)			Ben (n=6)	Mal (n=54)	
<i>ADC</i> _{mean}	77	1.37[.75-2.61]	.97[.74-2.57]	.082	55	1.28[.74-2.67]	1.20[.70-3.22]	.124	68	1.10[.73-1.66]	.94[.63-2.78]	.139
<i>ADC</i> _{skew}	88	.04[-1.61-1.29]	.90[0.26-1.18]	<.001	75	.11[-1.20-1.45]	0.59[-1.14-2.03]	<.001	93	.03[-.67-.28]	.91[-.17-2.05]	<.001
<i>ADC</i> _{kurt}	67	2.47[1.57-9.04]	3.09[2.62-3.33]	.139	52	3.03[1.72-11.96]	3.12[1.94-8.31]	.447	82	2.47[1.94-3.90]	4.23[2.40-9.69]	<.001
<i>ADC</i> _{stdev}	58	.16[.03-0.55]	.10[.03-.32]	.132	56	.20[.08-.85]	.22[.06-.52]	.358	88	.37[.25-.61]	.23[.11-.48]	.001

**ADC*_{mean}= mean apparent diffusion coefficient (x 10⁻³ mm²/s); *stdev*= standard deviation (x 10⁻³ mm²/s), *kurt*= kurtosis, *skew*= skewness,

Acc= accuracy, Ben= benign, Mal= malignant

*≤p25 equals the 25 percent smallest nodes, ≥p75 equals the 25 percent largest nodes and p25-75 equals all volumes in between.

Table 4. Per-region accuracies of all examined ADC parameters

		ADC			
		Mean ($\times 10^{-3}$ mm ² /s)	Skew	Kurt	Stdev ($\times 10^{-3}$ mm ² /s)
All n=241	Cut-off	1.11	0.38	2.95	0.22
	Acc	67.2%	83.4%	65.6%	58.9%
	n=140 Med [range] Ben	1.34[.73-2.67]	.06[-1.61-1.45]	2.79[1.54-11.96]	.19[.03-.85]
n=101	Med [range] Mal	1.04[.63-3.22]	.74[-1.14-2.05]	3.59[1.94-9.69]	.23[.03-.52]
Ing n=35	Cut-off	1.04	0.30	2.79	0.18
	Acc	74.3%	91.4%	68.6%	74.3%
	n=21 Med [range] Ben	1.16[.84-190]	.10[-.90-1.45]	2.69[1.57-4.81]	.13[.07-.23]
n=14	Med [range] Mal	.97[.63-1.67]	.99[.21-2.03]	3.37[2.58-8.31]	.20[.03-.48]
Il n=35	Cut-off	1.10	0.63	4.00	0.16
	Acc	71.4%	82.9%	71.4%	65.7%
	n=21 Med [range] Ben	1.19[.76-2.16]	.21[-1.20-1.45]	3.24[1.98-8.85]	.15[.77-.32]
n=14	Med [range] Mal	1.02[.65-2.20]	1.16[-.52-2.05]	4.37[2.82-8.64]	.22[.06-.39]
Retro n=38	Cut-off	1.42	0.46	2.90	0.20
	Acc	81.6%	89.4%	71.1%	71.1%
	n=26 Med [range] Ben	1.66[1.25-2.56]	-.05[-1.23-.75]	2.67[1.69-11.96]	.18[.11-.42]
n=12	Med [range] Mal	1.34[.79-3.22]	.84[-.39-1.89]	3.67[2.59-7.10]	.26[.18-.45]
Mes n=9	Cut-off	1.30	0.35	2.54	0.24
	Acc	77.8%	77.8%	88.9%	55.6%
	n=4 Med [range] Ben	1.46[.92-1.73]	-.002[-.33-.35]	2.53[1.74-3.89]	.29[.19-.42]
n=5	Med [range] Mal	1.23[.73-1.66]	.56[.11-1.43]	3.31[2.65-5.34]	.26[.13-.37]
Med n=32	Cut-off	1.60	0.28	2.45	0.23
	Acc	78%	78.1%	78.1%	59.4%
	n=12 Med [range] Ben	1.87[1.04-2.67]	.05[-.90-.54]	2.36[1.86-5.63]	.34[.15-.85]
n=20	Med [range] Mal	1.05[.75-2.78]	.56[-1.14-1.59]	3.69[1.99-6.35]	.24[.08-.39]
Ax n=48	Cut-off	0.91	0.22	3.24	0.22
	Acc	83.3%	87.5%	68.8%	62.5%
	n=35 Med [range] Ben	1.15[.73-2.61]	-.01[-1.61-.86]	2.86[1.54-9.04]	.21[.05-.69]
n=13	Med [range] Mal	.85[.67-1.32]	1.10[-.55-1.95]	4.30[2.39-9.69]	.24[.10-.43]
Cerv n=44	Cut-off	1.04	0.38	2.94	0.15
	Acc	65.9%	81.8%	70.4%	61.4%
	n=21 Med [range] Ben	1.21[.74-2.13]	.16[-1.33-1.29]	2.73[1.57-5.41]	.23[.03-.40]
n=23	Med [range] Mal	1.04[.72-1.70]	.66[.26-1.87]	3.40[1.94-7.77]	.19[.10-.52]

Stdev= standard deviation, Kurt= kurtosis, Skew= skewness; Acc= accuracy, Ben= benign, Mal= malignant, Ing= inguinal, Il= iliac, Retro= retroperitoneal, Mes= mesenteric, Med=mediastinal, Ax= axillary, Cerv= cervical

FIGURE HEADINGS

Figure 1. ROC curve of mean ADC and ADC texture parameters standard deviation (stdev), kurtosis and skewness.

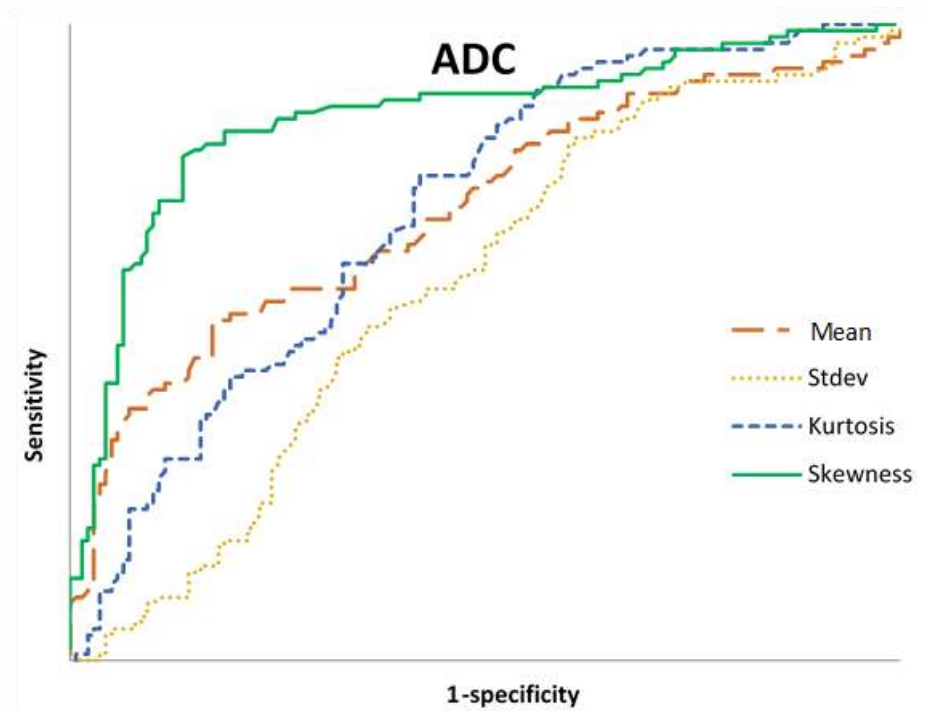


Figure 2. A) Illustration of a patient with stage II diffuse B-cell lymphoma, demonstrating a hyperintense malignant mass in the left cervical region (arrow) corresponding with an ADC histogram with an ADC_{mean} in the lower range, positive skew (high skewness) and a steep curve (high kurtosis). B) A different patient with a benign axillary lymph node, correlating with a higher ADC_{mean} value, a negative skew (low skewness), and a flatter shape (low kurtosis).

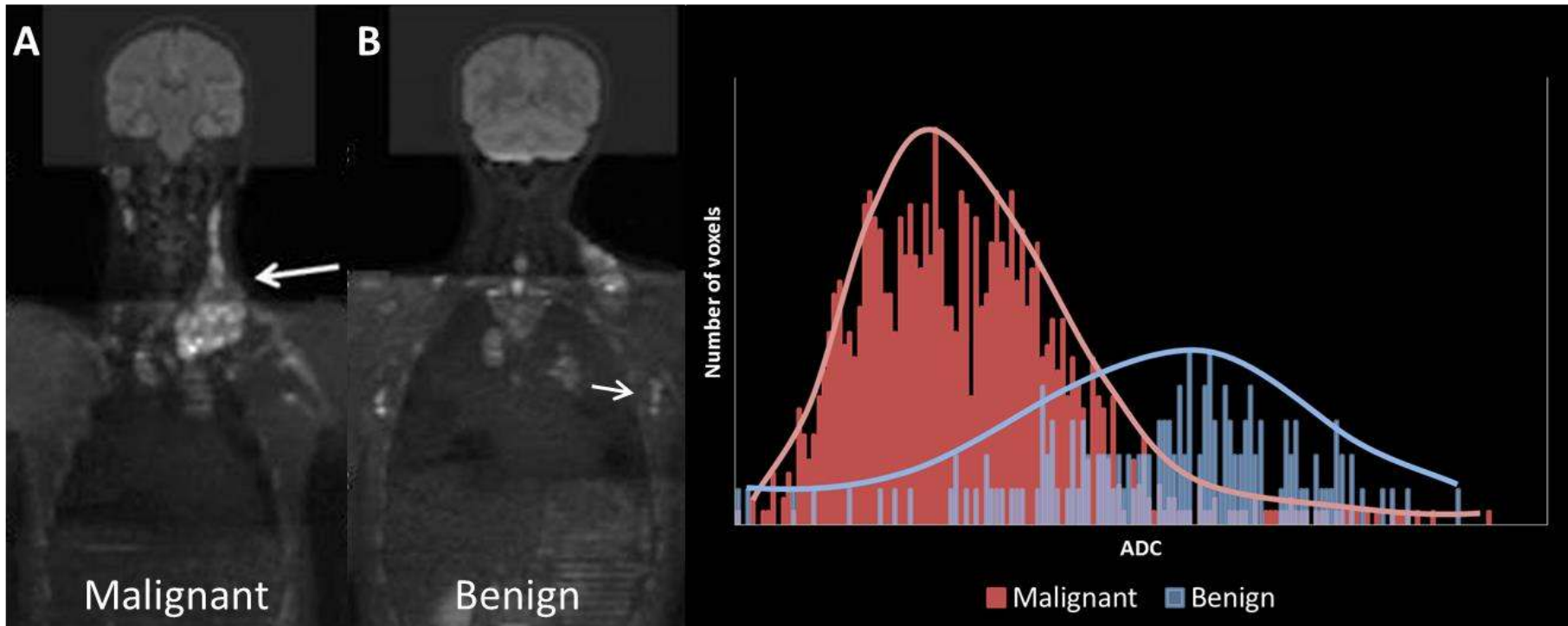


Figure 3. A) A 72-year old man with stage III Follicular lymphoma grade a. B) Involved mediastinal nodes demonstrated a higher ADC mean, larger standard deviation, more negative skew, and lower kurtosis than axillary nodes and C) inguinal nodes.

